Therapeutic vulnerability to PARP1,2 inhibition in *RB1*-mutant osteosarcoma

Georgia Zoumpoulidou
UCL Cancer Institute, University College London
Carlos Alvarez Mendoza
UCL Cancer Institute, University College London https://orcid.org/0000-0002-5972-0315
Caterina Mancusi
UCL Cancer Institute, University College London
Ritika-Mahmuda Ahmed
UCL Cancer Institute, University College London https://orcid.org/0000-0002-2866-3362
Milly Denman
UCL Cancer Institute, University College London
Christopher Steele
UCL Cancer Institute, University College London, London
Jiten Manji
UCL Cancer Institute, University College London
Nischalan Pillay
UCL Cancer Institute, University College London, London https://orcid.org/0000-0003-0579-4105
Sandra Strauss
University College London
Sibylle Mittnacht (s.mittnacht@ucl.ac.uk)
UCL Cancer Institute, University College London

Article

Keywords: Retinoblastoma tumour suppressor, RB1, osteosarcoma, PARP, PARP inhibitor sensitivity, targeted therapy, stratified therapy

Posted Date: February 5th, 2021

DOI: https://doi.org/10.21203/rs.3.rs-185226/v1

Version of Record: A version of this preprint was published at Nature Communications on December 1st, 2021. See the published version at https://doi.org/10.1038/s41467-021-27291-8.

Abstract

Loss-of-function mutations in the *RB1* tumour suppressor are key drivers in cancer, including osteosarcoma. *RB1* loss-of-function compromises genome-maintenance and hence could yield vulnerability to therapeutics targeting such processes. Here we demonstrate selective hypersensitivity to clinically-approved inhibitors of Poly-ADP-Polymerase1,2 inhibitors (PARPi) in RB1-mutated cancer cells including an extended panel of osteosarcoma-derived lines. PARPi treatment results in extensive cell death in *RB1*-mutated backgrounds and prolongs survival of mice carrying human *RB1*-mutated osteosarcoma grafts. PARPi sensitivity is not associated with canonical homologous recombination defect (HRd) signatures, which predict PARPi sensitivity in cancers with BRCA1,2 loss, but is accompanied by rapid activation of DNA replication checkpoint signalling, and active DNA replication is a prerequisite for sensitivity. Importantly, sensitivity in backgrounds with natural or engineered RB1 loss surpasses that seen in *BRCA*-mutated backgrounds where PARPi have established clinical benefit. Our work provides evidence that PARPi sensitivity extends beyond cancers identifiable by HRd and advocates PARP1,2 inhibition as a novel, personalised strategy for *RB1*-mutated osteosarcoma and other cancers.

Introduction

Biallelic mutations targeting *RB1* are prominently associated with difficult to treat cancers, including osteosarcoma.

Osteosarcoma is the most common primary human bone malignancy. More than half of cases arise in children and young adults, with disproportionate contribution to cancer death in these age groups [1]. Aggressive multimodal treatment involving combination chemotherapy substantially increase survival. However, less than 30% of patients diagnosed with metastatic disease show long-term response; and relapse and treatment associated toxicity in patients diagnosed with localised disease remain chief concerns [1–3] [4].

Emerging osteosarcoma genomics data reveal the prominent presence of deleterious mutations in the known tumour suppressors *TP53, RB1, RECQL4, BLM, and WRN. RB1* mutations are seen in 40–60% of sporadic osteosarcoma [5,6] [7] making it the second most commonly mutated gene in this disease after *TP53*. Studies of osteosarcoma genomic evolution invariably report RB1 mutations as early, truncal events [8] [9] and germline mutations in *RB1* increase the risk of osteosarcoma development [10], denoting a causal role of *RB1* defects during disease initiation. Notably, various sources, including a recent systematic review, report association of *RB1* mutation with poor prognosis including high risk of metastasis [11], paralleling observations in other cancers with *RB1* involvement [12] [13] and indicating a clear unmet clinical need in patients with *RB1*-mutant osteosarcoma.

While conventional combination chemotherapy has remained standard of care for osteosarcoma irrespective of presentation or genotype [3], targeted agents including multitargeted tyrosine kinase inhibitors show efficacy in early phase clinical trials and may offer additional options in relapsed disease,

albeit with cost of significant treatment-related toxicity [14]. Personalised, biomarker-informed opportunities have been identified by preclinical work for various gain-of-function events [5 7 15 5], indicating targeted, genome-informed treatment could provide future solutions in osteosarcoma. However, opportunities identified by the highly prevalent loss-of-function events, including *TP53* and *RB1*, have not been reported.

RB1 is a negative regulator of the cell cycle but has been ascribed other functions [16]. *RB1* defects in cells cause complex changes including anomalies in DNA double-strand-break (DDSB) repair [17 18 19] and mitotic fidelity [20]. Such DNA metabolic alterations raise the possibility that synthetic lethal opportunities may exist involving therapeutics known to interact with defective DNA repair or mitosis.

Based on assessment of an extended osteosarcoma-focused cell line panel, we here report selective sensitivity of *RB1*-mutant osteosarcoma to inhibitors of Poly-(ADP-Ribose)-Polymerase1,2 (PARPi). PARP1,2 enzymes have complex roles in DNA single-strand-break (DSSB) repair, transcription and replication [21]. PARP1,2 inhibition is selectively lethal in cancer with mutation in the *BRCA*1,2 tumour suppressors, causing HRd [22], and multiple PARPi have regulator-approval for the treatment of HRd and/or BRCA1,2 mutated ovarian, breast and pancreatic cancers, with recent FDA breakthrough status in castration-resistant prostate cancer [23 24].

We here document highly penetrant PARPi hypersensitivity following from *RB1* mutation, with dose-sensitivity comparable to that caused by BRCA1,2 mutation. We validate the involvement of *RB1* defects in this response and document single-agent PARPi efficacy in a preclinical model of *RB1*-mutant osteosarcoma. Our work proposes a novel genome-led strategy for treatment of osteosarcoma, involving stratified use of PARP1,2 targeting therapeutics.

Results

PARPi sensitivity in *RB1*-mutant osteosarcoma tumour cell lines.

To identify therapeutically exploitable vulnerability linked to deleterious *RB1* mutation we assessed the sensitivity of histiotype-matched cancer cell line pairs differing in *RB1* mutation status to clinical candidate agents that target DNA metabolic processes.

Day-5 viability assessments involving resazurin-reduction revealed consistent hypersensitivity to the PARPi olaparib in *RB1*-mutant compared to matched *RB1*-normal lines (Supplementary Fig. 1a-c). A strong association between olaparib sensitivity and *RB1* status extended to a poly-cancer cell line panel, with median area-under-the-curve (AUC) values significantly lower in *RB1*-mutant compared to *RB1*-normal lines (Supplementary Fig. 1d-f), indicative that *RB1* status in cancers is associated with, and may predict hypersensitivity to PARPi.

Significantly, the increased dose sensitivity to olaparib extended to a broad osteosarcoma-focussed cell panel (Fig. 1a), yielding a highly significant differential median sensitivity assessed using AUC values

(Fig. 1b) in lines with known *RB1*-mutant status and/or lacking detectable RB1 expression (Fig. 1m), compared to *RB1*-normal lines. Significantly, median sensitivity in the RB1-mutant group was comparable to that of the pancreatic cancer line Capan-1, known for profound PARPi sensitivity due to defective *BRCA2* [25] that we included to benchmark clinically relevant response levels.

Similar results were obtained using the clinically approved but structurally unrelated PARPi niraparib (Fig. 1c, d) and talazoparib (Fig. 1e, f). Both yielded significantly increased median sensitivity for the *RB1*-mutant compared to the *RB1*-normal osteosarcoma group, with sensitivities across the *RB1*-mutant group greater than, or closely matching that of *BRCA2*-mutated Capan-1 (Fig. 1b, d, f). High correlation coefficients and highly significant linear correlations were obtained comparing repeat assessments of the same PARPi (Pearson $r = 0.92$, $p < 0.0001$ for olaparib, Pearson $r = 0.98$, $p < 0.001$ for niraparib and talazoparib), (Supplementary Fig. 1g-i), indicating reliability of the analysis. Importantly, highly significant linear correlations were obtained comparing different PARPi, (Fig. 1g, h), indicating that their shared activity of targeting PARP1,2 underlies the sensitivity profiles observed.

A significant association between sensitivity and *RB1*-defect was also observed using veliparib, a PARPi that inhibits PARP1,2 catalysis but lacks the ability to trap PARP1,2 enzymes on damaged chromatin [26] [27], (Fig. 1i, k), with significant correlation comparing repeat assessments (Supplementary Fig. 1k). However, the differential in sensitivity was small and the inhibitor concentration required to affect viability high. While consistent with an increased dependency on PARP1,2 catalysis, these results indicate that PARP trapping may be an important mechanistic determinant for single agent potency in *RB1*-mutant osteosarcoma, as is known for *BRCA1,2* mutated cancers [22].

Clonogenic assays, scoring for the ability of cells to form colonies, confirmed selective PARPi hypersensitivity in *RB1*-mutant osteosarcoma for all three PARPi (Fig. 2a-k, raw data Supplementary Fig. 2a-c) with half maximal inhibitory concentrations (IC50) for *RB1*-mutant osteosarcoma matching or below that determined for *BRCA2*-mutant Capan-1, and differentials in median IC50 value comparing *RB1*-normal and *RB1*-mutant groups of 14-fold (olaparib), 5-fold (niraparib) and 8-fold (talazoparib) (Fig. 2c, f, i and Supplementary Table 1). Superior selectivity of olaparib over niraparib was previously observed in HRd cancers, and may relate to differences in off-target activity of these different agents [28].

Collectively the data provide evidence that *RB1* status is a predictor of single-agent PARPi sensitivity in osteosarcoma, with sensitivity levels comparable to that of BRCA2-mutant cells.

PARPi induced cell death in *RB1*-mutant osteosarcoma

To understand how PARPi act to reduce cell viability in RB1-defective osteosarcoma we performed time-lapse microscopy using medium containing SYTOX™ death-dye, which marks cell death. Treatment with olaparib yielded a concentration-dependent increase in death-dye incorporation compared to vehicle-treated controls (Fig. 3a, b) accompanied by widespread cytopathic effects (Fig. 3b) in *RB1*-mutant but not *RB1*-normal osteosarcoma lines.

Increased death-dye incorporation and cytopathic effects became evident 40 and 60 hours after PARPi addition. Statistics comparing death above vehicle (excess death) at 94–96 hours identified a highly significant differential between the *RB1*-mutant and *RB1*-normal group with a strong and significant inverse correlation between death and the IC50 for the respective lines, consistent with a link between olaparib-induced death and antiproliferative response (Fig. 3c, d).

Corroborative results were obtained using talazoparib or niraparib, with concentration-dependent death in *RB1*-mutant but not RB1-normal osteosarcoma, and similar time to onset (40 to 60 hours) regardless of PARPi used (Supplementary Fig. 3a-c). Together these results are consistent with an enhanced sensitivity to PARPi in *RB1*-mutant osteosarcomas and identify rapid cell death as a key consequence of PARPi exposure in osteosarcoma cells with this genetic defect.

PARPi sensitivity is a consequence of *RB1* deficiency

To investigate if selective PARPi sensitivity in *RB1*-mutant osteosarcomas is a consequence of RB1 loss, we depleted RB1 in *RB1*-normal osteosarcoma CAL72 using multiple *RB1*-targeting small-hairpin RNAs (shRNA) (Fig. 4a).

Clonogenic survival assessments revealed a significant increase in olaparib sensitivity of the various RB1-depleted lines compared to unmodified CAL72 or empty vector controls (Fig. 4b, c and Supplementary Fig. 4a), yielding IC50 values for the RB1-depleted group in the sub-micromolar range and a differential in median IC50 compared to controls of > 10-fold (Fig. 4d and Supplementary Table 2). Consistent results were obtained using niraparib (Fig. 4e-g, Supplementary Table 2 and Supplementary Fig. 4b) revealing significantly greater sensitivity in the RB1-depleted lines, with clear, albeit smaller differential in median IC50 between groups (> 5-fold), consistent with observations comparing naturally *RB1*-mutant and *RB1*-normal osteosarcoma lines.

Notably, time-lapse microscopy revealed a significant rise in cell death in RB1-depleted CAL72 compared to controls, that progressively increased with increasing olaparib (Fig. 4, i) or talazoparib (Fig. 4k, l) concentrations. Collectively, these data provide strong evidence that RB1 loss is causative and responsible for the increased hypersensitivity of *RB1*-mutant osteosarcomas to PARP1,2 inhibition.

Mechanism of PARPi sensitivity in *RB1*-mutated osteosarcoma

Since PARPi hypersensitivity in cancers is caused by BRCAness/HRd [29], we determined if RB1 loss may yield BRCAness/HRd. The inability of cells to recruit the DNA recombinase RAD51 to DDSBs is regarded an indicator of BRCAness/HRd [30 31]. We therefore quantified RAD51 recruitment in *RB1*-mutant osteosarcoma lines using ionising radiation (IR) to induce DDSBs (Fig. 5a-c). To benchmark response, we included HR and RAD51 recruitment defective Capan-1, and HR and RAD51 recruitment competent colorectal carcinoma HT29 cells.

We observed a significant DNA damage-dependent RAD51 recruitment, evidenced by increased numbers of cells with >15 RAD51 foci, and a significant increase in foci numbers per cell in all *RB1*-mutated osteosarcoma lines except one, LM7. LM7 have previously been reported as RAD51 recruitment defective [15] thought to be linked to reduced expression of multiple HR components. As expected, inability of DNA damage-dependent RAD51 recruitment was seen in Capan-1, while substantive gain in RAD51 positive cells and significant increase in foci numbers was seen in HR competent HT29 (Fig. 5a-c).

We also performed mutation spectrum analysis (Fig. 5d) using the publicly available whole genome sequence for nine of the osteosarcoma lines. HRd in cancers is associated with a signature of somatic mutations identified as single-base substitution signature 3 (SBS03), and presence of this signature provides a DNA-based measure of HRd [32]. While this analysis identified widespread presence of other signatures, evidence for exposure to HRd was only seen in one of three *RB1*-mutant lines. Notably, NY, the *RB1*-mutant line with HRd exposure, was RAD51 recruitment competent, indicative that exposure to HRd may either be historic, or caused by a mechanism downstream of RAD51 recruitment. Analysis of published osteosarcoma whole exome data [33] confirmed *RB1* defects are not significantly associated with HRd exposure (Supplementary Fig. 5). Namely, HRd exposure was not detectable in 5 of 10 tumours with *RB1* mutation and had no significant linkage to *RB1* mutational status.

Together these data argue that *RB1* defects in osteosarcoma do not cause HRd/ BRCAness and hence that PARPi sensitivity in *RB1*-mutant osteosarcoma is mechanistically distinct from and not explained by outright inability to engage HR-based DNA repair.

Platinum sensitivity in *RB1*-mutated osteosarcoma

PARPi sensitivity in *BRCA*1,2-mutated cancer is paralleled by hypersensitivity to platinum drugs, and platinum drug sensitivity is a predictor of BRCAness/HRd. Importantly, platinum drugs are an important component of clinical care in osteosarcoma. We therefore assessed if *RB1* status, that our work shows predicts PARPi sensitivity, might likewise predict platinum sensitivity.

However, assessment of response to cisplatin across the various osteosarcoma lines using clonogenic survival (Fig. 6a-c, Supplementary Fig. 6a, Supplementary Table 1) or day-5 viability (Supplementary Fig. 6b-c) revealed no significant difference in AUC or IC50 value distributions between groups. Notably, median sensitivities closely matched that for *BRCA2*-mutated, cisplatin-hypersensitive Capan-1 [34], indicating high platinum sensitivity across osteosarcoma lines, irrespective of *RB1* status and PARPi sensitivit

To assess if *RB1* defects could cause platinum sensitivity we made use of the RB1-depleted CAL72. While unmodified CAL72 had modest cisplatin sensitivity (Supplementary Table 2, IC50 > 1 μM), a significant and substantive sensitivity increase was seen in RB1-depleted CAL72, using clonogenic activity (Fig. 6d-f, Supplementary Table 2, Supplementary Fig. 6d) or day-5 viability (Supplementary Fig. 6e, f). Hence, although platinum sensitivity is widespread amongst the established osteosarcoma lines and here is not

predicted by *RB1* status, these latter data argue that *RB1* defects, alike *BRCA1,2* defects, increase platinum sensitivity.

PARPi activate DNA replication checkpoint response in *RB1*-mutant osteosarcoma

To begin to understand what causes the PARPi hypersensitivity in *RB1*-mutant cancer cells we assessed DDSB-damage response activation in *RB1*-mutant and RB1-normal osteosarcoma cell lines. PARP inhibition prevents the ligation of DSSBs and traps PARP complex on these lesions, leading to DDSB once cells move into S-phase, which cannot be appropriately resolved in PARPi sensitive cells with HRd [35 36].

To assess if DDSBs arise and may selectively accumulate in *RB1*-mutant cells, we measured the level of the DDSB repair histone marker γH2AX using immunohistochemistry (Fig. 7a, b and Supplementary Fig. 7a, b).

We observed a robust and significant rise in γH2AX-positive cells following treatment with PARPi olaparib in two different *RB1*-mutant osteosarcoma lines (Fig. 7a), seen within 2 hours but increasing with time of treatment. Signals in cells positive for γH2AX were confined to the cell nucleus with characteristic speckled appearance, comparable in distribution and intensity to those caused by IR (Supplementary Fig. 7a). No significant increase in γH2AX-positive cells compared to vehicle treatment was observed in two *RB1*-normal osteosarcoma lines albeit γH2AX-positive cells significantly increase following IR exposure (Fig. 7a and Supplementary Fig. 7b). Importantly, PARPi treatment induced significant γH2AX positivity following RB1 ablation in CAL72 (Fig. 7b). No significant increase was seen in CAL72 that expressed irrelevant control shRNA targeting the human haemoglobin A (HBA) or were unmodified. These results indicate that canonical DDSB damage signalling ensues in response to PARP inhibition of *RB1*-mutant osteosarcoma, with direct evidence that RB1 loss is a prerequisite and causative in this response.

γH2AX may signify activation of distinct DNA damage response pathways, notably, ATM, activated in response to DDSB, or ATR, activated in response to DNA replication impairment. To delineate which of these pathways may be activated we scored for the activating phosphorylation of checkpoint kinase CHK1, targeted by ATR, and CHK2, selectively linked to ATM signalling [37]. Quantitative immunoblot analysis revealed a prominent increase in CHK1 phosphorylation following PARPi treatment of the *RB1*-mutated OHSN (Fig. 7c, d), surpassing that observed in response to IR in the same cells (Fig. 7d). Using the same lysates, only a modest phosphorylation of CHK2 was observed, despite strong phosphorylation of CHK2 in response to IR (Fig. 7c, e). PARPi treatment failed to increase phosphorylation of CHK1 or CHK2 in the *RB1*-normal CAL72 (Fig. 7f-h), consistent with the lack of substantive γH2AX positivity in these cells. However, prominent CHK1 activation arose in RB1-ablated CAL72 (Fig. 7m-o) compared to unmodified CAL72, run in parallel (Fig. 7i-l). Hence, PARPi treatment elicits signalling consistent with replication checkpoint activation in *RB1*-mutant cells, indicative that DNA replication fork impairment is a key event arising in these cells.

Requirement of DNA replication for PARP inhibitor toxicity in *RB1*-mutant cells

To address if DNA replication is a requirement for toxicity of PARP inhibition to unfold in *RB1*-mutated osteosarcoma, we assessed whether preventing this process prevents PARPi-induced death. We cultured *RB1*-mutated OHSN in medium containing excess thymidine to halt DNA replication during olaparib treatment (Fig. 8a). Subsequently we quantified cell death measuring SYTOX™ death-dye uptake using time-lapse imaging. OHSN cells treated with olaparib whilst under thymidine-induced DNA replication block showed striking, highly significant reduction in cell death rate, compared to cycling cells. Yet death response was restored to levels similar to that in cycling cells when cells were released from the thymine-induced block prior to olaparib addition, ($^{ns}p= 0.1736$) (Fig. 8b-c). These results provide direct evidence that ongoing DNA replication is required for death to unfold in response to PARPi treatment in *RB1*-mutated osteosarcoma.

PARP inhibitor yields robust single-agent activity in *in vivo* preclinical models of *RB1*-mutant human osteosarcoma

Given the substantive single-agent PARPi sensitivity of *RB1*-mutated osteosarcoma cells in cell-based experiments we assessed whether the single-agent sensitivity extends to *in vivo* models of human osteosarcoma. To this end we generated xenografts of *RB1*-mutated OHSN in immunodeficient NRG mice. Following tumour formation, mice were randomised and treated once daily for three successive 5-day periods with either vehicle or talazoparib at 0.33 mg/kg (Fig. 8d, e).

Treatment using this schedule was well tolerated, with no adverse impact on weight (Supplementary Fig. 8) or other adverse effects observeable. However, a highly significant reduction in tumour growth, apparent after a single 5-day cycle (**$p < 0.01$), was seen in the talazoparib-treated compared to vehicle-treated mice. Notably, while tumours in vehicle-treated mice progressed rapidly (Fig. 8d), reaching the maximally allowable size by 22 days, none of the tumours in talazoparib-treated mice progressed to this level within that time. Importantly, and although dosing of talazoparib was discontinued on day 20, > 70% of the tumours in talazoparib-treated mice remained within allowable limits at day 26, when observation was terminated (Fig. 8e). These data provide evidence that the single-agent PAPRi sensitivity observed in cell-based assay translates into substantive single-agent preclinical anti-tumour activity, yielding reduced disease progression and extended survival in mice carrying human *RB1*-mutant osteosarcoma xenografts.

Discussion

Our work identifies PARP inhibition as a synthetic vulnerability and therapeutic opportunity for RB1-mutated osteosarcoma with additional evidence that deleterious *RB1* mutation may be a biomarker for clinically relevant PARP1,2 inhibitor sensitivity in other cancers. PARPi are in current clinical use, with notable effect on quality of life and overall survival in multiple cancers [38]. Their existing clinical utility highlight the imminent opportunity for clinical translation of the results we here report.

Patient selection in current clinical applications relies on evidence of HRd in cancer tissue [39 40]. However, genomic or functional evidence for frank HRd was not detectable or significantly associated with RB1 loss in cancer, which excludes these cancers from treatment using current eligibility criteria.

Our work documents that enforced RB1 loss causes clinically meaningful sensitivity (i.e. sensitivity akin to that seen in *BRCA1,2*-defective Capan-1) in an otherwise PARPi insensitive osteosarcoma line, providing proof of concept for a direct role of RB1 loss in the selective PARPi sensitivity observed. The lack of frank HRd in cancer cell lines with RB1 loss raises questions as to the mechanism that underlies their sensitivity. Our work positively identifies PARPi trapping and active DNA replication as mechanistic prerequisites for sensitivity, paralleling observations in cancers with HRd [26 36]. These observed similarities argue for a shared inability of cancers with HRd or RB1 loss to avert the lethal consequence of replication fork obstruction, caused by trapped PARP complex and known to underly PARPi inhibitor sensitivity caused by HRd.

Published data propose a role of RB1 in HR, entailing E2F1-dependent recruitment of chromatin remodelling activity to sites of DNA damage [18], albeit, the scale of HRd arising through this mechanism has not been assessed. It is conceivable that localised HRd arising within subgenomic contexts, although not detected in genome wide mutation spectrum analysis, could cause a synthetic lethality interaction between RB1 loss and PARP inhibition. Other evidence links chromatin processes, including defective DNA cohesion and chromatin remodelling to PARPi sensitivity [41 42]. Defects in these processes are known to result from RB1 loss [43], which in turn could explain the observed sensitivity phenotype.

While our work advocates the use of PARPi in *RB1*-mutated osteosarcoma, comprehensive preclinical validation, including how PARPi should be best integrated into the current management of osteosarcoma, will be of likely paramount importance to ensure clinical benefit.

PARPi are rapidly moving into first-line clinical use in patients with HRd ovarian cancers and considerable efforts are underway to extend their use to other cancers. Most pertinent to the work reported here is the planned assessment of PARPi within the paediatric MATCH study (NCT03233204), a large scale precision medicine trial in children, adolescents, and young adults with advanced cancers including osteosarcoma, with use of *BRCA1,2* mutation or HRd for patient selection. The highly penetrant hypersensitivity in *RB1*-mutant osteosarcoma cells shown here combined with the currently limited options in patient with such cancers, advocates expansion of assessment to include RB1-mutated disease.

Material And Methods

Cell lines, Chemicals and Antibodies. The osteosarcoma tumour cell lines were described previously [15]. PARPi and cisplatin were purchased from Selleck Chemicals. Antibodies and shRNAs are detailed in Supplementary Materials. Mutation spectrum analysis was as described [32].

Assessment of drug response. Drug sensitivity was assessed in 96-well plates based on resazurin-reduction five days following drug addition. Clonogenic survival assesssments and immunofluorescence staining were performed as described [44]. Time-lapse microscopy was performed in 96-well plates as described in [45] using an IncuCyte ZOOM live cell analysis system (Essen Bioscience). For cell cycle analysis, cells were fixed in 70% ethanol, stained using propidium iodide and analysed using flow cytometry. Immunoblot analysis used whole-cell protein extracts prepared by lysis of cells into 0.1% SDS, 50 mM TRIS-HCL, pH 6.8, containing protease and phosphatase inhibitors (ThermoFisher Scientific, UK). *In vivo* experiments were carried out under UK Home Office regulations in accordance with the Animals (Scientific Procedures) Act 1986 and according to United Kingdom Coordinating Committee on Cancer Research guidelines for animal experimentation [46] with Animal Welfare Ethical Review Body (AWERB) approval. Tumour growth was assessed twice weekly using digital callipers. Assessments were terminated in accordance with AWERB guidelines.

Statistical Analysis. Statistical hypothesis testing was performed using Microsoft Excel or GraphPad Prism. Statistical tests used are named within the text. Differences with $p < 0.05$ were considered statistically significant.

Comprehensive method and material information is provided under Supplementary Materials.

Declarations

Data Availability

The authors declare that the data support the findings of this study are available within the Supplementary information or from the authors upon reasonable requests.

Authors contribution:

GZ, NP, SJS and SM contributed to the design of experiments and strategy; SM lead the project; GZ and SM wrote the manuscript; GZ, CA-M, CM, R-MA, MD, and CDM performed components of the experimental work and analyzed associated data; CDS performed the bioinformatics-based mutation signature analysis; JM assisted with microscopy and high-content data analysis

Declaration of interest

The authors do not declare any competing or conflict of interest. The funders had no role in design of the study, the collection, analysis, and interpretation of the data, the writing of the manuscript, or the decision to submit the manuscript for publication.

Acknowledgement:

The work was supported by grants from Children with Cancer UK. GZ and CA-M and MD were supported by Children with Cancer UK (ref.17–244), with additional support through philanthropic giving by charities

aid foundation account A80105053. CM was supported through a Cancer Research UK studentship (ref.C416/A23233). SJS was funded in part by NIHR UCLH Biomedical Research Centre.

References

1 Casali, P. G. et al. Bone sarcomas: ESMO-PaedCan-EURACAN Clinical Practice Guidelines for diagnosis, treatment and follow-up. *Ann Oncol* **29**, iv79-iv95, doi:10.1093/annonc/mdy310 (2018).

2 Isakoff, M. S., Bielack, S. S., Meltzer, P. & Gorlick, R. Osteosarcoma: Current Treatment and a Collaborative Pathway to Success. *J Clin Oncol* **33**, 3029-3035, doi:10.1200/JCO.2014.59.4895 (2015).

3 Gorlick, R. & Khanna, C. Osteosarcoma. *J Bone Miner Res* **25**, 683-691, doi:10.1002/jbmr.77 (2010).

4 Smeland, S. et al. Survival and prognosis with osteosarcoma: outcomes in more than 2000 patients in the EURAMOS-1 (European and American Osteosarcoma Study) cohort. *Eur J Cancer* **109**, 36-50, doi:10.1016/j.ejca.2018.11.027 (2019).

5 Perry, J. A. et al. Complementary genomic approaches highlight the PI3K/mTOR pathway as a common vulnerability in osteosarcoma. *Proc Natl Acad Sci U S A* **111**, E5564-5573, doi:10.1073/pnas.1419260111 (2014).

6 Kovac, M. et al. Exome sequencing of osteosarcoma reveals mutation signatures reminiscent of BRCA deficiency. *Nat Commun* **6**, 8940, doi:10.1038/ncomms9940 (2015).

7 Behjati, S. et al. Recurrent mutation of IGF signalling genes and distinct patterns of genomic rearrangement in osteosarcoma. *Nat Commun* **8**, 15936, doi:10.1038/ncomms15936 (2017).

8 Negri, G. L. et al. Integrative genomic analysis of matched primary and metastatic pediatric osteosarcoma. *J Pathol* **249**, 319-331, doi:10.1002/path.5319 (2019).

9 Brady, S. W. et al. The Clonal Evolution of Metastatic Osteosarcoma as Shaped by Cisplatin Treatment. *Mol Cancer Res* **17**, 895-906, doi:10.1158/1541-7786.MCR-18-0620 (2019).

10 Picci, P. Osteosarcoma (osteogenic sarcoma). *Orphanet J Rare Dis* **2**, 6, doi:10.1186/1750-1172-2-6 (2007).

11 Ren, W. & Gu, G. Prognostic implications of RB1 tumour suppressor gene alterations in the clinical outcome of human osteosarcoma: a meta-analysis. *Eur J Cancer Care (Engl)* **26**, doi:10.1111/ecc.12401 (2017).

12 Backlund, L. M., Nilsson, B. R., Liu, L., Ichimura, K. & Collins, V. P. Mutations in Rb1 pathway-related genes are associated with poor prognosis in anaplastic astrocytomas. *Br J Cancer* **93**, 124-130, doi:10.1038/sj.bjc.6602661 (2005).

13 Bhateja, P. et al. Retinoblastoma mutation predicts poor outcomes in advanced non small cell lung cancer. *Cancer Med* **8**, 1459-1466, doi:10.1002/cam4.2023 (2019).

14 Tian, Z., Niu, X. & Yao, W. Receptor Tyrosine Kinases in Osteosarcoma Treatment: Which Is the Key Target? *Front Oncol* **10**, 1642, doi:10.3389/fonc.2020.01642 (2020).

15 Holme, H. et al. Chemosensitivity profiling of osteosarcoma tumour cell lines identifies a model of BRCAness. *Sci Rep* **8**, 10614, doi:10.1038/s41598-018-29043-z (2018).

16 Dick, F. A., Goodrich, D. W., Sage, J. & Dyson, N. J. Non-canonical functions of the RB protein in cancer. *Nat Rev Cancer* **18**, 442-451, doi:10.1038/s41568-018-0008-5 (2018).

17 Cook, R. et al. Direct involvement of retinoblastoma family proteins in DNA repair by non-homologous end-joining. *Cell Rep* **10**, 2006-2018, doi:10.1016/j.celrep.2015.02.059 (2015).

18 Velez-Cruz, R. et al. RB localizes to DNA double-strand breaks and promotes DNA end resection and homologous recombination through the recruitment of BRG1. *Genes Dev* **30**, 2500-2512, doi:10.1101/gad.288282.116 (2016).

19 Jiang, Y., Yam, J. C., Tham, C. C., Pang, C. P. & Chu, W. K. RB Regulates DNA Double Strand Break Repair Pathway Choice by Mediating CtIP Dependent End Resection. *Int J Mol Sci* **21**, doi:10.3390/ijms21239176 (2020).

20 Manning, A. L., Longworth, M. S. & Dyson, N. J. Loss of pRB causes centromere dysfunction and chromosomal instability. *Genes Dev* **24**, 1364-1376, doi:10.1101/gad.1917310 (2010).

21 Ray Chaudhuri, A. & Nussenzweig, A. The multifaceted roles of PARP1 in DNA repair and chromatin remodelling. *Nat Rev Mol Cell Biol* **18**, 610-621, doi:10.1038/nrm.2017.53 (2017).

22 Lord, C. J. & Ashworth, A. PARP inhibitors: Synthetic lethality in the clinic. *Science* **355**, 1152-1158, doi:10.1126/science.aam7344 (2017).

23 Curtin, N. J. & Szabo, C. Poly(ADP-ribose) polymerase inhibition: past, present and future. *Nat Rev Drug Discov* **19**, 711-736, doi:10.1038/s41573-020-0076-6 (2020).

24 Gourley, C., Miller, R. E., Hollis, R. L. & Ledermann, J. A. Role of Poly (ADP-Ribose) Polymerase inhibitors beyond BReast CAncer Gene-mutated ovarian tumours: definition of homologous recombination deficiency? *Curr Opin Oncol* **32**, 442-450, doi:10.1097/CCO.0000000000000660 (2020).

25 McCabe, N. et al. BRCA2-deficient CAPAN-1 cells are extremely sensitive to the inhibition of Poly (ADP-Ribose) polymerase: an issue of potency. *Cancer Biol Ther* **4**, 934-936, doi:10.4161/cbt.4.9.2141 (2005).

26 Murai, J. et al. Trapping of PARP1 and PARP2 by Clinical PARP Inhibitors. *Cancer Res* **72**, 5588-5599, doi:10.1158/0008-5472.CAN-12-2753 (2012).

27 Hopkins, T. A. et al. Mechanistic Dissection of PARP1 Trapping and the Impact on In Vivo Tolerability and Efficacy of PARP Inhibitors. *Mol Cancer Res* **13**, 1465-1477, doi:10.1158/1541-7786.MCR-15-0191-T (2015).

28 Antolin, A. A. et al. The kinase polypharmacology landscape of clinical PARP inhibitors. *Sci Rep* **10**, 2585, doi:10.1038/s41598-020-59074-4 (2020).

29 Lord, C. J. & Ashworth, A. BRCAness revisited. *Nat Rev Cancer* **16**, 110-120, doi:10.1038/nrc.2015.21 (2016).

30 Farmer, H. et al. Targeting the DNA repair defect in BRCA mutant cells as a therapeutic strategy. *Nature* **434**, 917-921, doi:10.1038/nature03445 (2005).

31 Dedes, K. J. et al. PTEN deficiency in endometrioid endometrial adenocarcinomas predicts sensitivity to PARP inhibitors. *Sci Transl Med* **2**, 53ra75, doi:10.1126/scitranslmed.3001538 (2010).

32 Alexandrov, L. B. et al. The repertoire of mutational signatures in human cancer. *Nature* **578**, 94-101, doi:10.1038/s41586-020-1943-3 (2020).

33 Behjati, S. et al. Recurrent mutation of IGF signalling genes and distinct patterns of genomic rearrangement in osteosarcoma. *Nature Communications* **8**, 15936, doi:10.1038/ncomms15936 (2017).

34 Sakai, W. et al. Secondary mutations as a mechanism of cisplatin resistance in BRCA2-mutated cancers. *Nature* **451**, 1116-1120, doi:10.1038/nature06633 (2008).

35 Pommier, Y., O'Connor, M. J. & de Bono, J. Laying a trap to kill cancer cells: PARP inhibitors and their mechanisms of action. *Sci Transl Med* **8**, 362ps317, doi:10.1126/scitranslmed.aaf9246 (2016).

36 Michelena, J. et al. Analysis of PARP inhibitor toxicity by multidimensional fluorescence microscopy reveals mechanisms of sensitivity and resistance. *Nat Commun* **9**, 2678, doi:10.1038/s41467-018-05031-9 (2018).

37 Smith, J., Tho, L. M., Xu, N. & Gillespie, D. A. The ATM-Chk2 and ATR-Chk1 pathways in DNA damage signaling and cancer. *Adv Cancer Res* **108**, 73-112, doi:10.1016/B978-0-12-380888-2.00003-0 (2010).

38 Pilie, P. G., Gay, C. M., Byers, L. A., O'Connor, M. J. & Yap, T. A. PARP Inhibitors: Extending Benefit Beyond BRCA-Mutant Cancers. *Clin Cancer Res* **25**, 3759-3771, doi:10.1158/1078-0432.CCR-18-0968 (2019).

39 Ledermann, J. A. Extending the scope of PARP inhibitors in ovarian cancer. *Lancet Oncol* **20**, 470-472, doi:10.1016/S1470-2045(19)30019-1 (2019).

40 Miller, R. E. et al. ESMO recommendations on predictive biomarker testing for homologous recombination deficiency and PARP inhibitor benefit in ovarian cancer. *Ann Oncol* **31**, 1606-1622, doi:10.1016/j.annonc.2020.08.2102 (2020).

41 Bajrami, I. et al. Genome-wide profiling of genetic synthetic lethality identifies CDK12 as a novel determinant of PARP1/2 inhibitor sensitivity. *Cancer Res* **74**, 287-297, doi:10.1158/0008-5472.CAN-13-2541 (2014).

42 Bailey, M. L. et al. Glioblastoma cells containing mutations in the cohesin component STAG2 are sensitive to PARP inhibition. *Mol Cancer Ther* **13**, 724-732, doi:10.1158/1535-7163.MCT-13-0749 (2014).

43 Manning, A. L. et al. Suppression of genome instability in pRB-deficient cells by enhancement of chromosome cohesion. *Mol Cell* **53**, 993-1004, doi:10.1016/j.molcel.2014.01.032 (2014).

44 Zhang, C. et al. Signalling involving MET and FAK supports cell division independent of the activity of the cell cycle-regulating CDK4/6 kinases. *Oncogene* **38**, 5905-5920, doi:10.1038/s41388-019-0850-2 (2019).

45 Goncalves, T. et al. Selective Elimination of Osteosarcoma Cell Lines with Short Telomeres by Ataxia Telangiectasia and Rad3-Related Inhibitors. *ACS Pharmacology & Translational Science* **3**, 1253-1264, doi:10.1021/acsptsci.0c00125 (2020).

46 Workman, P. et al. UKCCCR guidelines for the welfare of animals in experimental neoplasia. *Lab Anim* **22**, 195-201, doi:10.1258/002367788780746467 (1988).

Figures

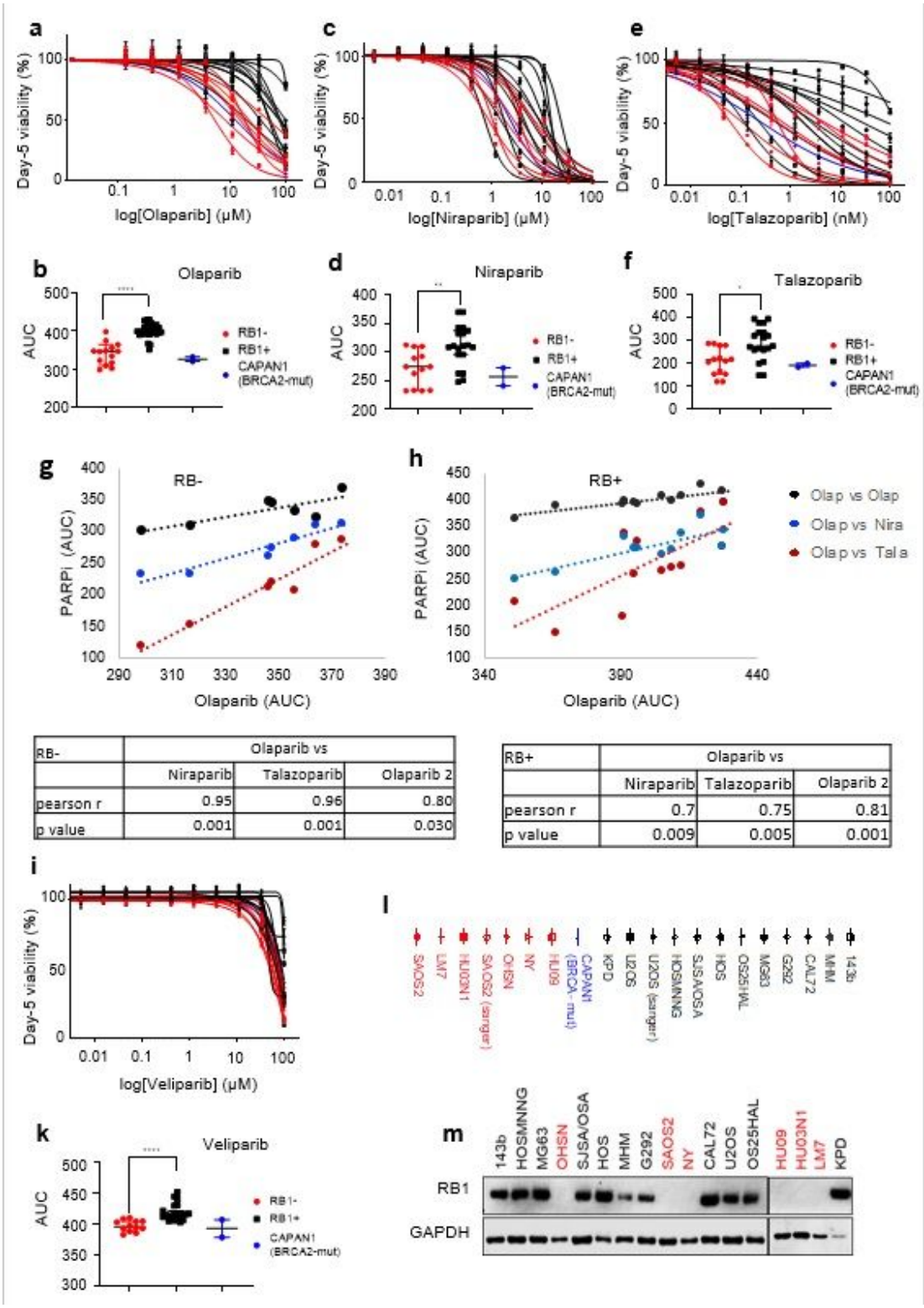

RB-	Olaparib vs		
	Niraparib	Talazoparib	Olaparib 2
pearson r	0.95	0.96	0.80
p value	0.001	0.001	0.030

RB+	Olaparib vs		
	Niraparib	Talazoparib	Olaparib 2
pearson r	0.7	0.75	0.81
p value	0.009	0.005	0.001

Figure 1

Differential PARPi sensitivities in RB1-mutant and RB1-normal osteosarcoma-derived tumour cell lines. Cell seeded in 96-well plates were treated with PARPi at concentrations as indicated. Cell viability was determined 5 days following inhibitor addition using resazurin-reduction. a, c, e) Concentration-response curves for a) Olaparib, c) Niraparib, or e) Talazoparib. Data are from one representative experiment. Data points represent the averages of three replicate samples relative to the DMSO-treated controls. RB1-

mutant (red), RB1-normal osteosarcoma-derived line (back), BRCA2-mutant pancreatic ductal carcinoma-derived Capan-1 (blue). b, d, f) Scatter plots depicting AUC values deduced from dose response curves for RB1-mutant (red) or RB1-normal (black) osteosarcoma lines or BRCA2-mutant Capan-1 (blue), treated with b) Olaparib, d) Niraparib, or f) Talazoparib, summarising results for two or more individual experiments. Bars depict median and 95% confidence interval (CI), * $p<0.05$, ** $p<0.01$, **** $p<0.0001$, using a 2-sided Mann-Whitney test. g, h) Pearson product moment correlation measuring the strength of a linear association between AUC data for olaparib and AUC data for talazoparib (red), niraparib (blue) or a 2nd olaparib dataset (black), g) RB1-mutant osteosarcoma lines and h) RB1-normal osteosarcoma lines. Tables showing Pearson's correlation coefficient and p values. i) Concentration-response curve for PARPi Veliparib depicting averages of three replicate samples relative to the DMSO-treated controls for one representative experiment, and k) Scatter plot depicting AUC values summarising data for two individual experiments. Bars depict median and 95% confidence interval (CI), **** $p<0.0001$, using a 2-sided Mann-Whitney test. l) Symbols and names for cell lines used. RB1-mutant (red), RB1-normal osteosarcoma-derived line (back), BRCA2-mutant pancreatic ductal carcinoma-derived Capan-1 (blue). m) Immunoblotting analysis assessing the expression of RB1 in osteosarcoma-derived cell lines. GAPDH was used as loading control.

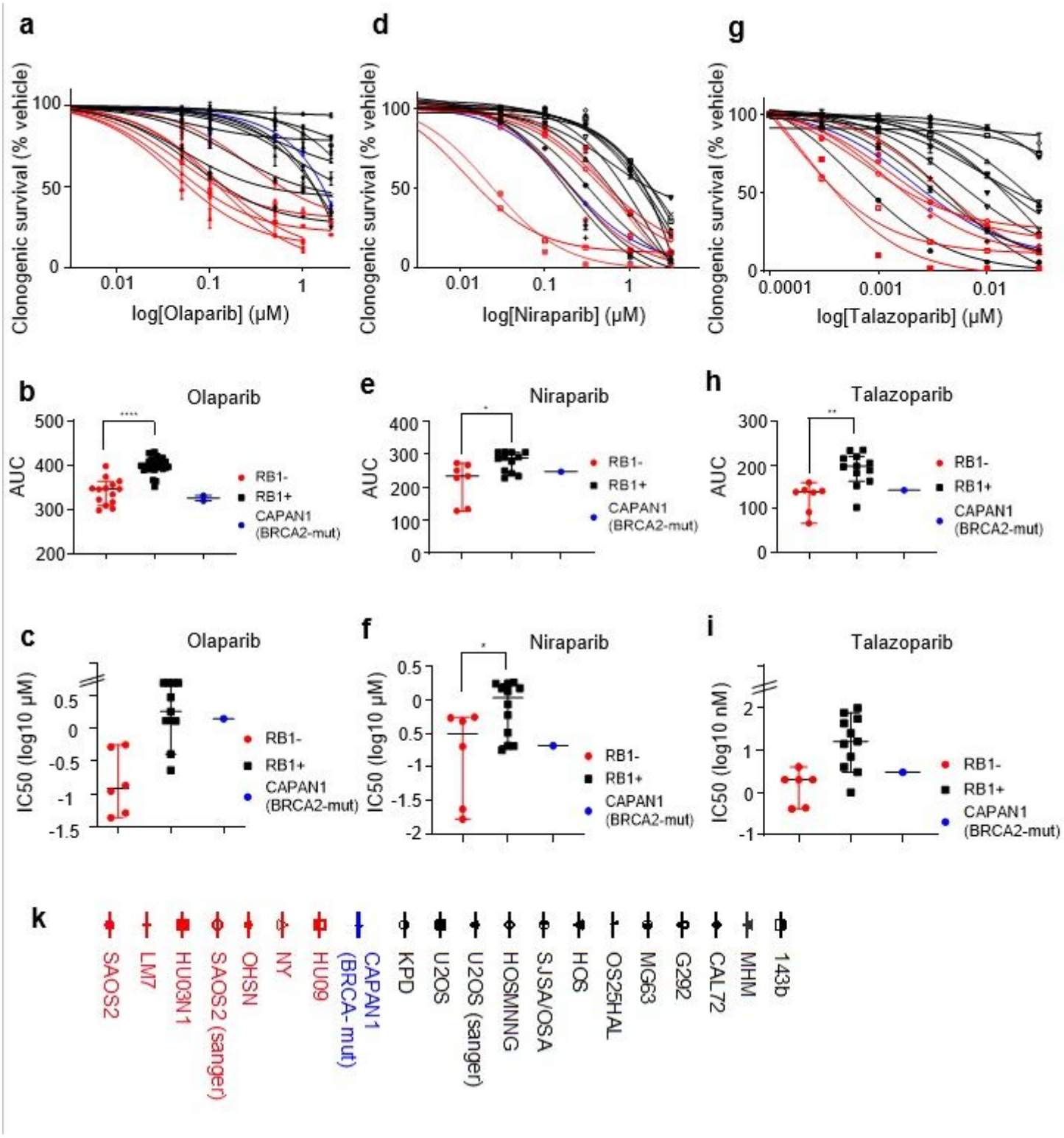

Figure 2

Effect of PARP inhibition on clonogenic survival. Cells were seeded into 6-well plates in the presence of vehicle (DMSO) or increasing concentrations of PARP inhibitors. Colonies arising were stained using crystal violet dye. Clonogenic survival was quantified using dye extraction. a, d, g) Concentration-response curves for RB1-mutant (red) or RB1-normal (black) osteosarcoma and BRCA2-mutant Capan-1 (blue) after treatment with a) Olaparib, d) Niraparib, or g) Talazoparib. Data reflect the mean +/-SD of

duplicate wells for one representative experiment. b, e, h) Scatter plots depicting AUC values for RB1-mutant or RB1-normal osteosarcoma lines and BRCA2-mutant Capan-1 treated with b) Olaparib, e) Niraparib, or h) Talazoparib summarising data from one or more experiments. Bars depict median and 95% CI. *p<0.05, **p<0.01, ****p<0.0001 calculated using 2-sided Mann-Whitney tests. c, f, i) Scatter plots depicting IC50 values deduced from dose response data in b, e and h. Bars depict median and 95% CI. k) Symbols and names for cell lines used.

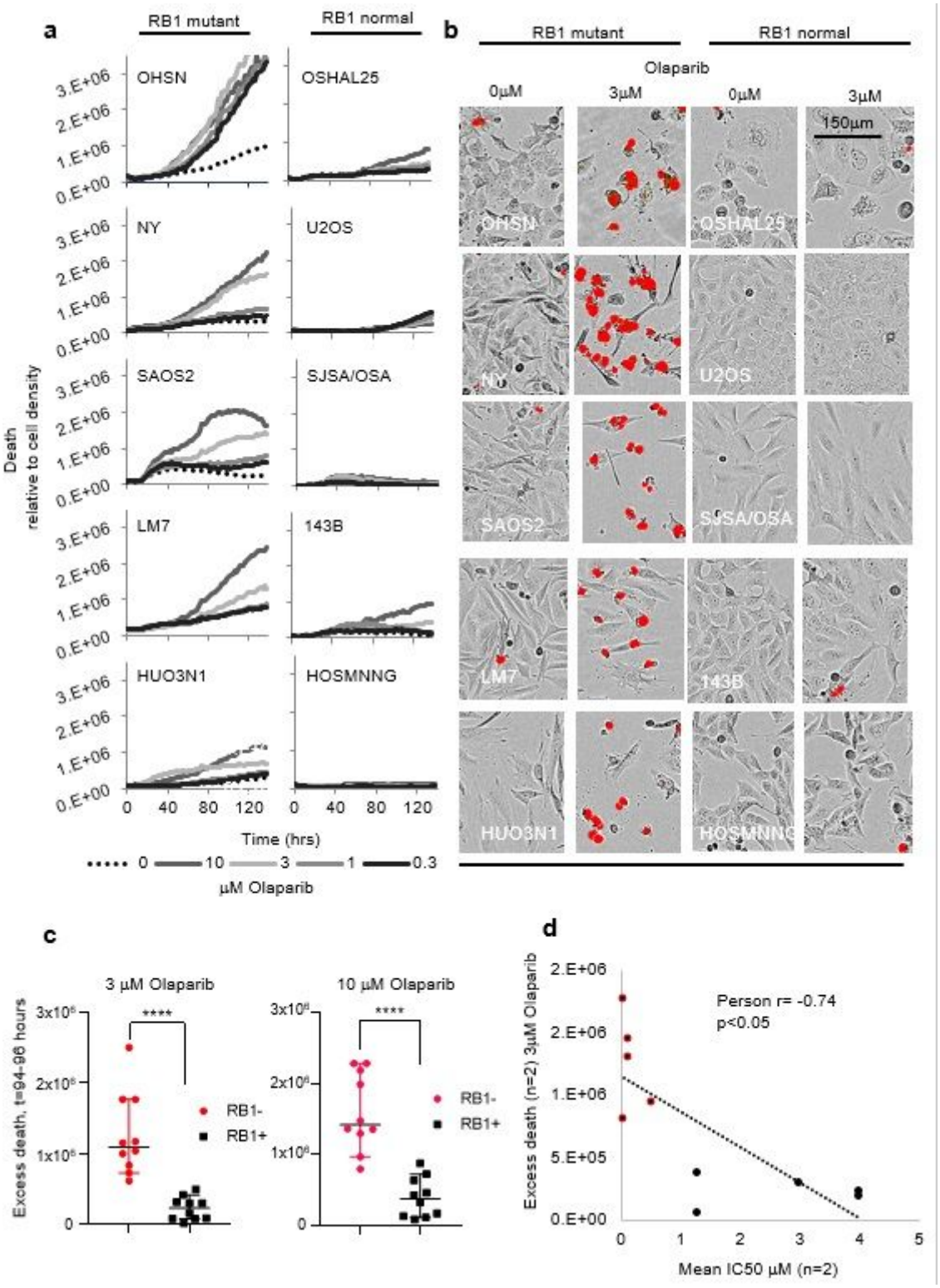

Figure 3

Cellular effects of PARPi treatment. RB1-mutant and RB1-normal osteosarcoma lines seeded in 96 well plates were treated with PARPi olaparib at concentrations indicated, then subjected to time-lapse microscopy in the presence of SYTOXTM death-dye. Images were taken every two hours, recording phase contrast and death-dye fluorescence. a) Death-dye incorporation over time relative to cell density in RB1-mutant (left) and RB1-normal (right) osteosarcoma cancer lines. b) Raw images 96 hours post inhibitor addition, depicting phase contrast superimposed with death-dye fluorescence. c) Mean death above vehicle (excess death) 94 to 98 hours after olaparib addition. Olaparib concentration were as indicated. d) Pearson product moment correlation measuring the strength of a linear association between mean excess death at 94 to 98 hours and IC50 determined using clonogenic assays for the same cell lines. Pearson's correlation coefficient (Pearson r) and p value are indicated Data represent one exemplary experiment (a, b) or are cumulative for two independent experiments (c, d) ****$p<0.0001$, 2-sided Mann-Whitney test.

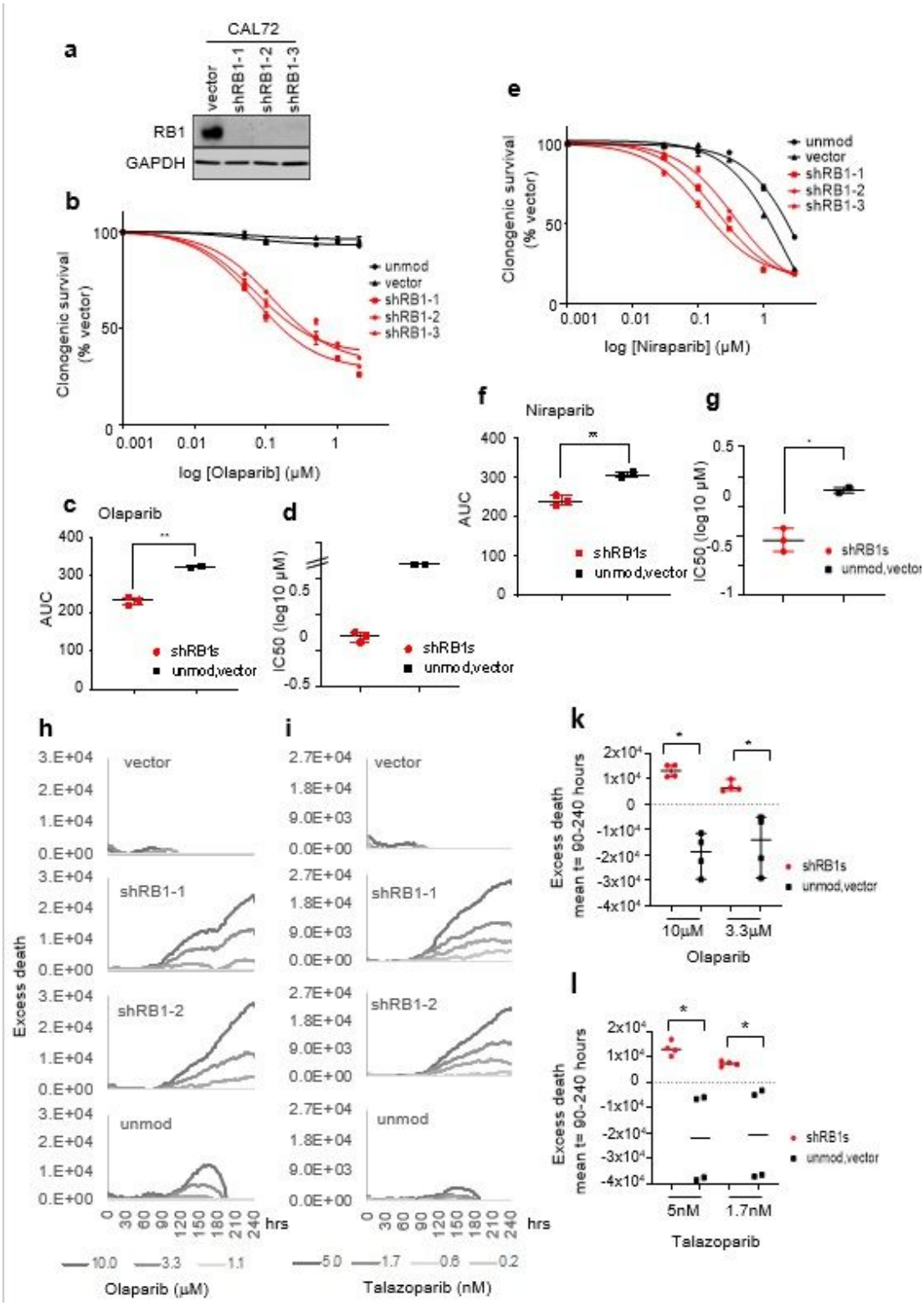

Figure 4

PARPi response in RB1-normal osteosarcoma following RB1 depletion. RB1-normal osteosarcoma CAL72 cells were infected with lentivirus vector encoding different RB1-targeting shRNAs (shRB1-1, shRB1-2 or shRB1-3) or empty vector backbone (vector) or were left unmodified (unmod.) a) Immunoblot analysis documenting RB1 expression. GAPDH was used as a loading control. b-g) Clonogenic survival analysis depicting concentrations-effect curves, AUC scatter plots and IC50 data for cells treated with b, c, d)

olaparib or e, f, g) niraparib. CAL72 with modifications as indicated were seeded into 6 well plates and treated with PARPi at concentrations as indicated. Data reflect the mean +/-SD of duplicate wells for one representative experiment. Bars depict median and 95% CI. *p<0.05, **p<0.01, calculated using 2-sided Mann-Whitney tests. h-l) Time-lapse microscopy assisted fate assessment. CAL72 modified as indicated were treated with PARPi and monitored for death-dye incorporation over time. h, i) Excess death above vehicle over time, k, l) Mean excess death between 90 and 240 hours. Data represent one exemplary experiment (h, i) or are cumulative for two independent experiments (k, l) *p<0.05, calculated using 2-sided Mann-Whitney tests. Bars depict median and 95% CI.

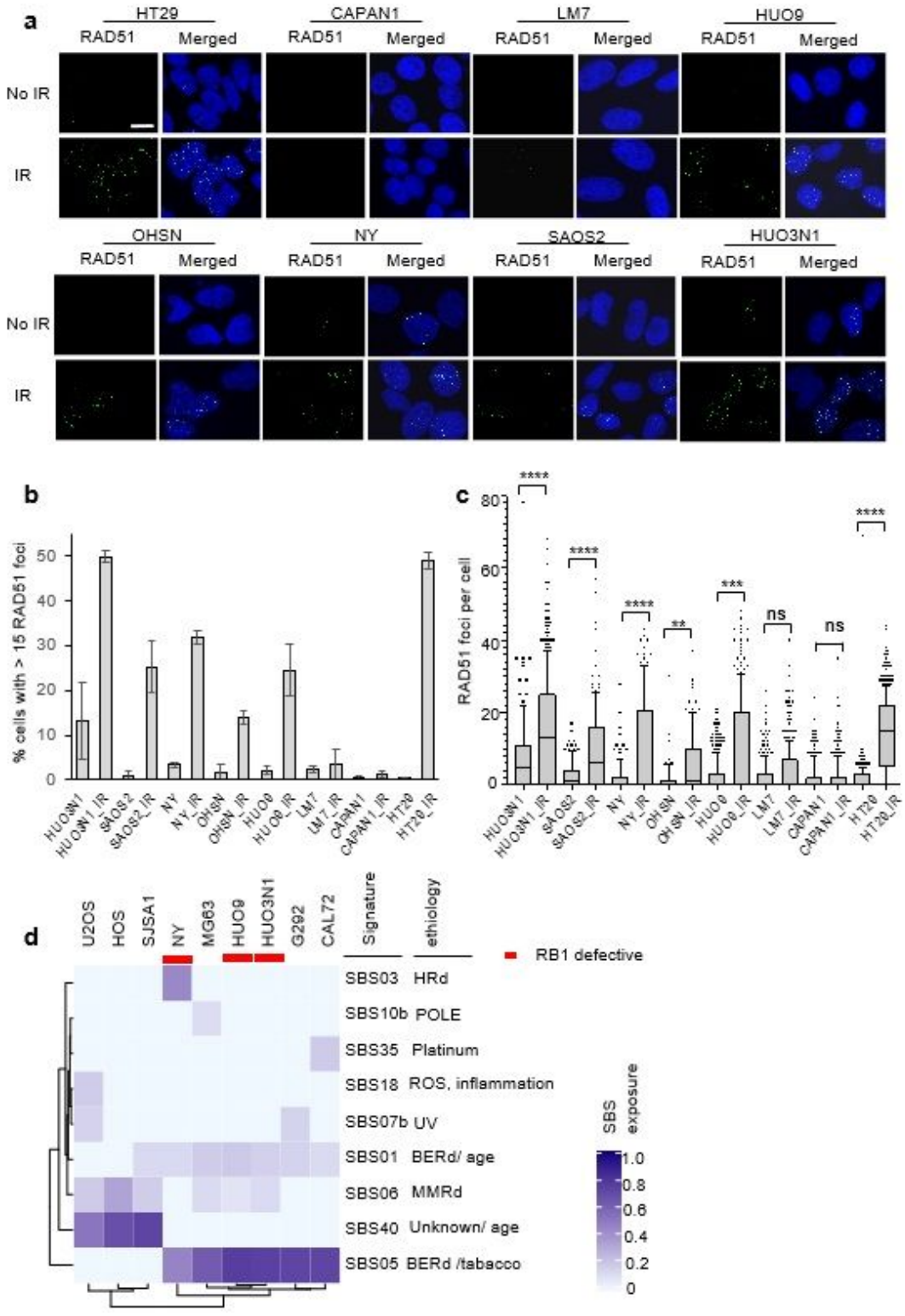

Figure 5

HR capability in RB1-defective osteosarcoma cell lines. a-c) DNA damage-dependent RAD51 recruitment in RB1-mutant osteosarcoma cell lines. Cells grown on glass coverslips were irradiated (4Gy) or left untreated. Cells were fixed 1 hour following IR, subjected to immunostaining for RAD51 and nuclear foci scored using confocal microscopy. A minimum of 100 cells per line were assessed across two or more experiments. a) Raw confocal images. Scale bar, 10 μm. RAD51 foci (green) and merged with images

counter-stained for DNA using DAPI (blue). b) Bar chart depicting quantitation of RAD51 nuclear foci. Bars depict the % of cells with >15 nuclear foci (mean ±SEM, n>2 experiments). c) Box and Whiskers plot (±95%CI) depicting RAD51 foci numbers per cell. nsp>0.05, **p<0.01, ***p<0.001, ****p<0.0001 using a Kruskal-Wallis test with Sidak's multiple comparisons correction d) Single base substitution mutational signature analysis. Whole genome sequencing data for cell lines were downloaded from the Broad Institute's Cancer Cell Line Encyclopedia. Signature analysis used SigProfilerMatrixGenerator, shown with associated etiology prediction. Etiology terms; Homologous recombination defect (HRd), Base excision repair defect (BERd), apolipoprotein B mRNA editing enzyme (APOBEC).

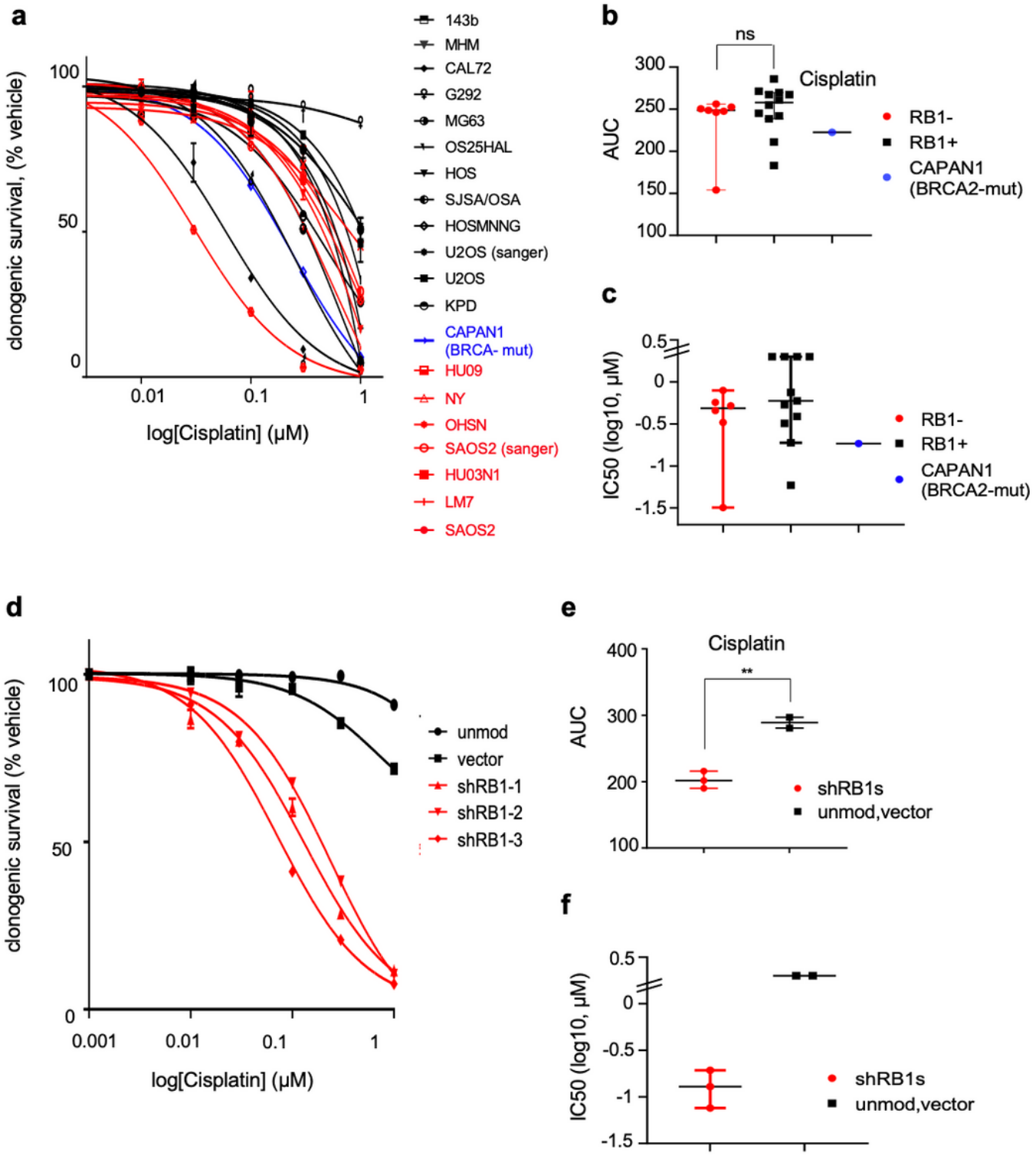

Figure 6

Platinum sensitivity in RB1-mutated osteosarcoma. Cells seeded into 6-well plates were cultured in the presence of vehicle (DMSO) or increasing concentrations of cisplatin. Colonies arising were stained using crystal violet dye. Clonogenic survival was quantified using dye extraction. a-c) Platinum response in RB1-mutant (red) or RB1-normal (black) osteosarcoma and BRCA2-mutant Capan-1 (blue). a) concentration-response curve and scatter plots depicting b) AUC value comparison and c) log IC50

values, deduced from the concentration- response data in a). Data reflect the mean +/-SD of duplicate wells for one representative experiment. Bars in scatter plots (b, c) depict median (±95%CI), nsp>0.05, calculated using 2-sided Mann-Whitney test. d-f) RB1-normal osteosarcoma CAL72 cells transduced with lentivirus vector encoding different RB1-targeting shRNAs (shRB1-1, shRB1-2 or shRB1-3) (red) or empty vector backbone (vector) or left unmodified (unmod) (black). d) concentration-response curve and scatter plots depicting e) AUC value comparison and f) log IC50 values, deduced from the concentration-response data in d). Data reflect the mean +/-SD of duplicate wells for one representative experiment. Bars in scatter plots (e, f) depict median (±95%CI), **p<0.01, calculated using 2-sided Mann-Whitney test.

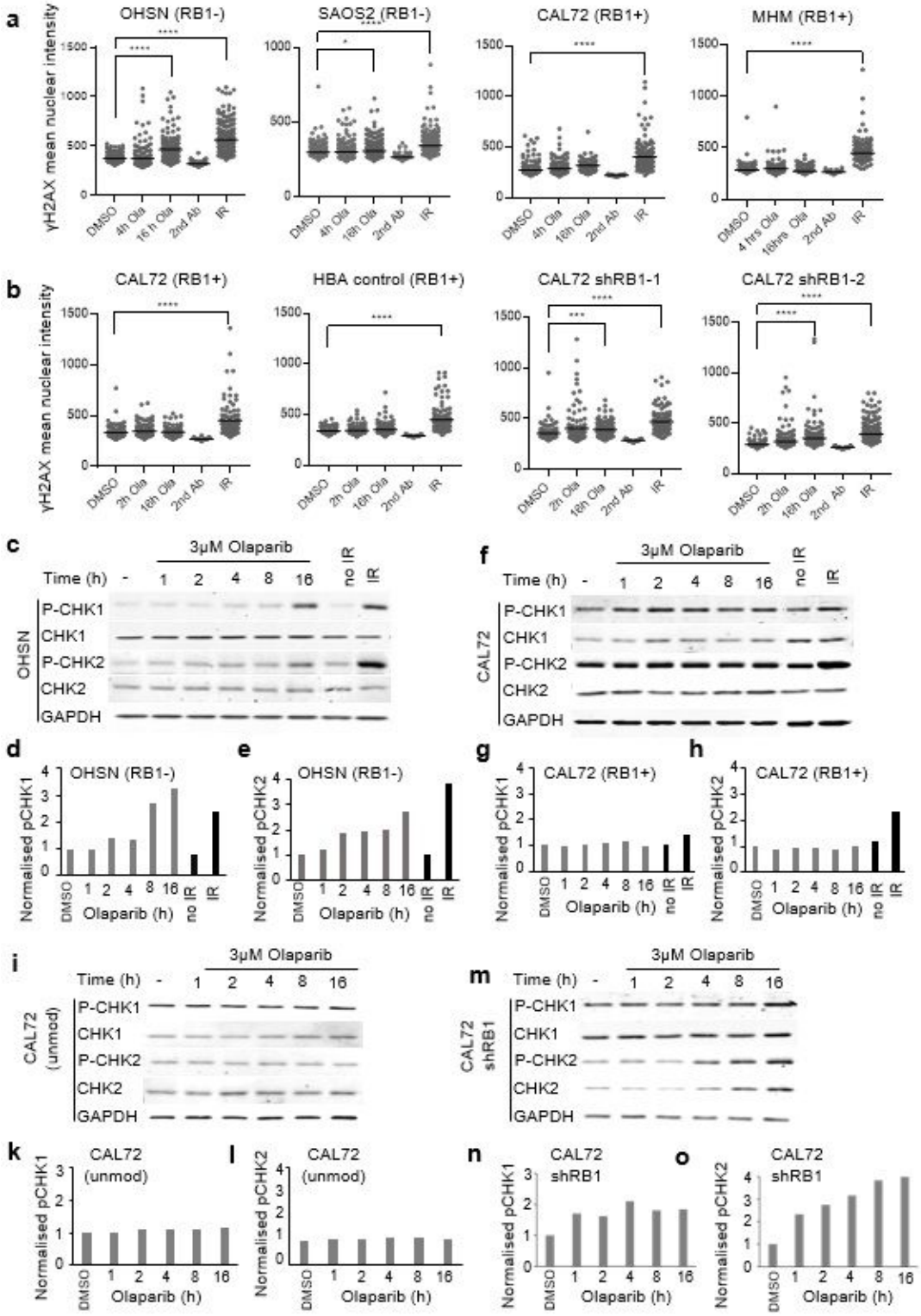

Figure 7

Effect of PARP inhibition on DNA damage response in cells with different RB1 status. a-b) DDSB repair signalling assessed using anti-phospho (Ser139) H2AX (γH2AX) immunofluorescence, a) in osteosarcoma cells with different RB1 status, or b) in RB1-normal osteosarcoma CAL72 transduced with lentivirus vector encoding RB1- or irrelevant control hemoglobin (HBA)-targeting shRNA. Cell lines after treatment with DMSO, 3μM olaparib, or 2.5 Gy of IR. Cells were exposed to olaparib for 2 or 4 or 16 hours

or allowed to recover for 1 hour after IR. Scatter blots report distribution and mean for samples from one representative experiment, respectively. Data shown are representative for one of two or more independent experiments. c-o) DDSB repair checkpoint signalling assessed using phosphor(Ser345)-CHK1 (pCHK1) and phosphor(Thr68)-CHK2 (pCHK2) quantitative immunoblot analysis in c-e) RB1-mutant, f-h) RB1-normal osteosarcoma cells lines and i-o) Unmodified RB1-normal CAL72 or with shRNA-mediated RB1 depletion. Cell lines after treatment with vehicle, 3μM olaparib, or 2.5 Gy IR and exposed to olaparib for 2 or 4 or 16 hours or allowed to recover for 1 hour after IR. GAPDH was used as loading control. CHK1 and CHK2 denote immunoblot signals for pan-CHK1 and -CHK2. Bar graphs represent pCHK signals relative to GAPDH. Data shown are representative for one of two or more independent experiments.

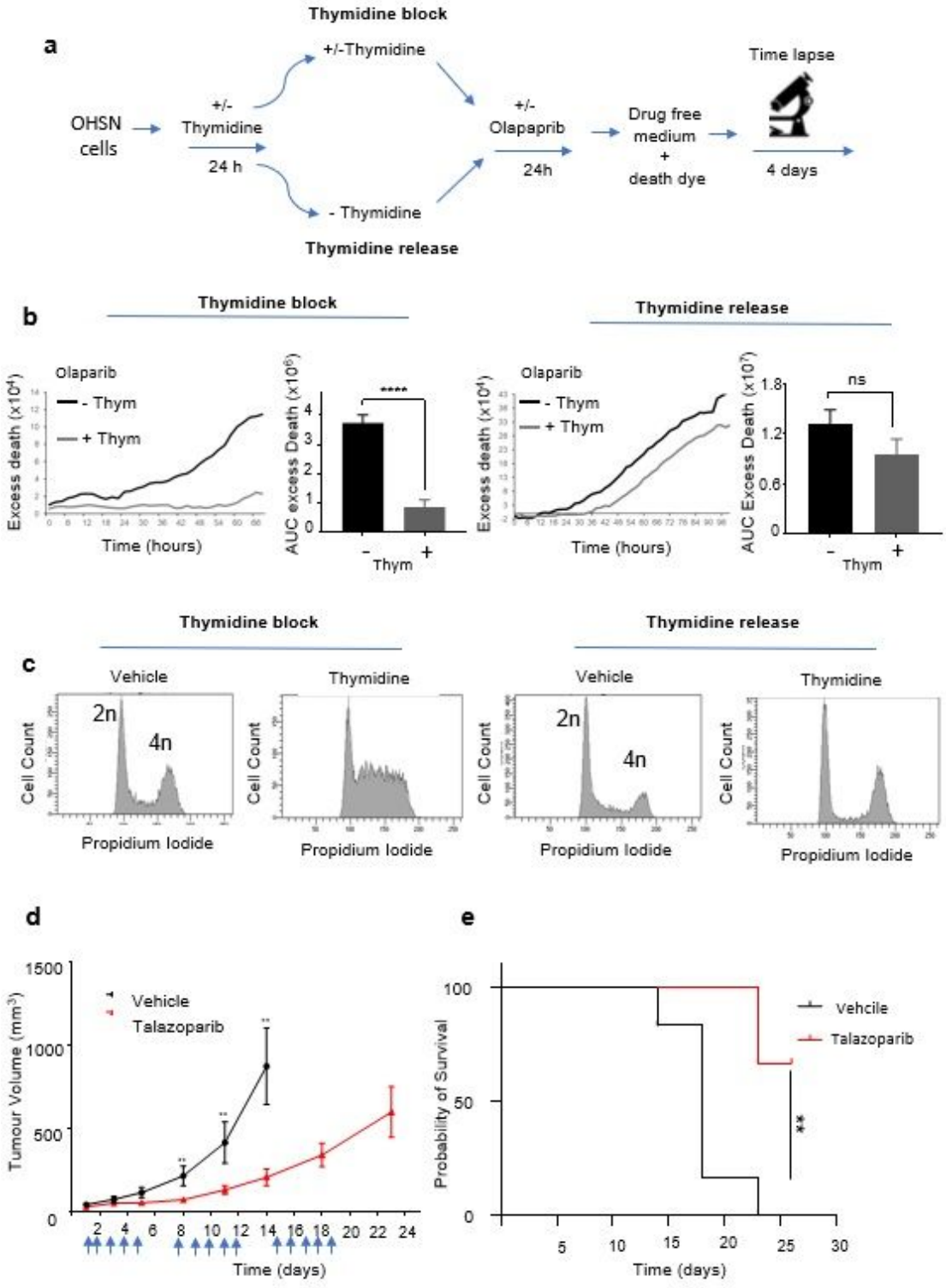

Figure 8

Effect of DNA replication impairment and tumour response in vivo. a-c) PARPi sensitivity following DNA replication perturbation a) Experiment design for assessing the role of DNA replication in PARPi sensitivity. RB1-mutant OHSN seeded in 96 well plates were treated as indicated, then subjected to time-lapse microscopy in the presence of SYTOXTM death-dye. b) Death assessed SYTOXTM death-dye incorporation. Raw traces depicting excess death above vehicle for one representative experiment, and

bar graphs depicting AUC values summarizing excess death over vehicle (±SEM) for n=5 independent experiments. nsp>0.05, ****p<0.0001, calculated using unpaired student t test. c) Cell cycle profiles documenting the effect of thymidine treatment on cell cycle progression. Cells seeded in parallel 6 well plates were treated as for b), then analysed using flow cytometry at 32 hour. Data shown are from one representative experiment. d-e) Tumour response to single agent PARPi treatment. NRG (NOD.Cg-Rag1tm1Mom Il2rgtm1Wjl/Szj) mice carrying OHSN tumour xenografts were treated daily (5 times per week) with the PARPi talazoparib at 0.33 mg/kg, or vehicle for 3 weeks (n=6 per group). d) Tumour volumes over time (mean ±SEM, n = 6), measured at the indicated time points. Arrows indicate dosing schedule of PARPi or vehicle. e) Kaplan-Meier survival analysis of NRG mice bearing tumours treated with talazoparib or vehicle. **p < 0.01 calculated using a log rank (Mantel-Cox) test.

Supplementary Files

This is a list of supplementary files associated with this preprint. Click to download.

- Zoumpoulidouetal.supplement.docx